

# We are IntechOpen, the world's leading publisher of Open Access books Built by scientists, for scientists

6,900

Open access books available

185,000

International authors and editors

200M

Downloads

Our authors are among the

154

Countries delivered to

TOP 1%

most cited scientists

12.2%

Contributors from top 500 universities



WEB OF SCIENCE™

Selection of our books indexed in the Book Citation Index  
in Web of Science™ Core Collection (BKCI)

Interested in publishing with us?  
Contact [book.department@intechopen.com](mailto:book.department@intechopen.com)

Numbers displayed above are based on latest data collected.  
For more information visit [www.intechopen.com](http://www.intechopen.com)



# Confocal Laser Scanning Microscopy of Living Cells

Alexey Moshkov

## Abstract

Living cells are distinguished in their ability to keep the structural stability in the changing environment by means of energy supply. Understanding the mechanisms of energy conversion is impossible without knowledge of the physiological processes involved. This question is addressed to confocal laser scanning microscopy (CLSM) that has become a leader among the group of light microscopy method. The high resolution in CLSM images is reached without deconvolution procedures. Linear characteristics of its variable parameters are important for quantitative image analysis. These properties of CLSM are indispensable in the study of mitochondrial membrane potential (MMP) using fluorescent dyes. Lipophilic rhodamine dyes freely pass the plasma membrane and accumulate in the mitochondria according to electrical potential difference. CLSM images of TMRE (tetramethylrhodamine, ethyl ester)-stained U937 cells were analyzed by standard image processing procedures in ImageJ software. These procedures allow the creation of mask, applying it to original image. Average fluorescence intensity in selected regions was used as a measure of MMP changes during phytohemagglutinin treatment. This value was decreased by 34% after 2 h of lectin treatment. Some cells after mitogenic stimulation completely lost MMP. Deregulation of mitochondrial calcium handling and changes of cytoplasmic monovalent ion concentration are considered as mechanisms of MMP decrease during lymphocyte stimulation.

**Keywords:** confocal microscopy, mitochondrial membrane potential, image processing, image analysis, phytohemagglutinin, lymphocyte stimulation

## 1. Introduction

Before cultured cells were available, the main objects of cell physiology were nerve and blood cells. The study of giant axons showed that excitability and irritability are the most important properties of living cells. Russian physiologist E. Bauer used these properties to affirm the principle of “stable nonequilibrium” [1]. This principle explains that in the changing environment, living systems maintain their structural stability through energy supply. Instead of “energy,” however, he uses the term “work” performed by system against equilibrium. Physiological implication of this principle was found upon the study of nonequal redistribution of  $\text{Na}^+$  and  $\text{K}^+$  ions in cuttlefish neuron during impulse propagation [2].

Physiological studies of living cells are always done in conjunction with light microscopy methods. Later these methods got resolution sufficient to study cell structures in molecular scale. The maximum resolution that allows observation of hexagonal pattern on diatom algae is reached in basic microscopy by shutting the

condenser [3]. Near-field scanning optical microscopy (NSOM) overcomes the diffraction limit by using optical fiber for both illumination and scanning [4]. NSOM was able to visualize small antibody-labeled domains on the plasma membrane of living human skin fibroblasts [5]. The small thickness of these cells uses conventional epi-fluorescence microscopy to study the mitochondrial membrane potential (MMP) [6, 7] using the protocol of automated image analysis of mitochondrial shape originally tested by confocal microscopy [8, 9]. The same functionality but greater performance resides in the method of imaging flow cytometry. The method allows fluorescence quantification using spot masks that are created independently on pixel intensity. This method was applied for the characterization of MMP changes involved in the malignant transformation of cancer stem cells. MMP together with such parameters as glucose uptake, superoxide-anion production, and mitochondria mass served as indicator of tumorigenesis [10].

Besides using CCD camera in conventional fluorescence microscopy, video microscopy suggests built-in image processing algorithms that cause inadvertent effect on pixel intensity, but with additional calibration procedure, absolute intensities are also measurable [11]. Instead of these algorithms, conventional microscopy uses deconvolution to improve the quality of images as in confocal microscopy [12]. For example, deconvolution was applied to wide-field microscopy images to resolve DNA replication units that are studied only by electron and structured illumination microscopy [13]. Unlike these later methods, confocal and classical light microscopy possesses the ability to study these structures in the living cells.

Discrimination of depth is a property of confocal microscopy that relies to confocal diaphragm [14] and can be checked by measuring the point spread function (PSF), which is defined as the image of a single point [15]. To see the changes on the image of real object, which contains convoluted PSFs, is impossible unless deconvolution is applied [12]. Special image processing algorithm is also applied in confocal microscopy for quantitative fluorescence analysis. This algorithm was applied in quantitative studies of mitochondrial  $[Na^+]$  ( $[Na^+]_m$ ) and  $Ca^{2+}$  ( $[Ca^{2+}]_m$ ) and mitochondrial pH ( $pH_m$ ) in MDCK cells stained with one of the ion-sensitive dyes [16–18]. Obtaining information about cellular organelles such as mitochondria requires creation of mask.

The same analytical approach was applied for the study of MMP changes caused by phytohemagglutinin (PHA) treatment in histiocytic lymphoma U937 cells. The image of TMRE-stained cells was used for both creating the mask and obtaining quantitative data. The value of average intensity obtained from masked image is independent of the wide variation of MMP. Therefore, this image can serve as a measure of MMP. To consider the effect of large mitochondrial depolarization that occurs in cells after PHA treatment, data were presented as integrated density divided by the number of cells on the image.

PHA is a lectin that stimulates growth and division of lymphocytes in the process known as transformation [19]. Previous studies using indirect isotopic method have not found considerable MMP change during mitogenic stimulation [20]. At the same time, lectins are affecting all known metabolic pathways. Early response in lymphocytes to PHA treatment includes stimulation of glycolysis [21], activation of pentose-phosphate cycle [22], and activation of pyruvate dehydrogenase (PDH) [23] that is a key enzyme to connecting glycolysis and citric acid cycle.

## **2. Principles of confocal laser scanning microscopy (CLSM)**

The history of CLSM began when Marvin Minsky include in his patent letter the scheme with epi-illumination with two pinholes that play the same role as in “double focusing” scheme which have already been tested with a stage-scanning

device [24]. Historical information and many technical details are not covered in the present paper but can be found in an encyclopedia article written by Amos and colleagues [14]. From a biological point of view, the development of CLSM began in 1987 when microscopes with laser beam deflection system were able to scan living kidney epithelium cells [25] and spinal cord neurons [26].

The development of CLSM ranging from 1987 to 1995 is distinctive by exponential rise of citations for the query “microscopy AND confocal” (**Figure 1**). At this period, the number of studies retrieved by the query “microscopy NOT confocal” shows a rather decelerating trend. In 1995, the number of confocal microscopy studies started to grow linearly, while many microscopic studies remain unpublished. The second period ended with the new millennium when linear trend of CLSM publications was accompanied by extensive growth of other microscopic studies. The third period is therefore noticeable by concomitant development of all microscopic methods. During this period, confocal microscopy constitutes one sixth of microscopic papers. Indeed, this share would be greater if query is restricted only to cytological area. It can be concluded that the first period caused a 10-year delay in the development of other microscopical methods, while the second period caused its rapid growth.

Ideal confocal microscope has detector pinhole that is small enough to suppress the diffraction in emission light path. This made its resolution equally dependent from excitation and emission light paths [14]. Lateral resolution of real confocal microscope is determined by the illuminating pinhole that participates in the formation of PSF [15]. Therefore, lateral resolution of confocal microscope is given by formula

$$\text{FWHM}_{\text{lateral}} = \frac{0.51\lambda_{\text{ex}}}{NA} \tag{1}$$

where FWHM is the distance between the points on distribution where its intensity is half of that of the peak intensity,  $\lambda_{\text{ex}}$  is the wavelength of excitation light, and NA is the numerical aperture of objective. At  $NA = 1.42$  and  $\lambda_{\text{ex}} = 488 \text{ nm}$ , lateral resolution of confocal microscope is determined as  $0.175 \text{ }\mu\text{m}$ , while at  $\lambda_{\text{ex}} = 561 \text{ nm}$ , it reduced to  $0.2 \text{ }\mu\text{m}$ .

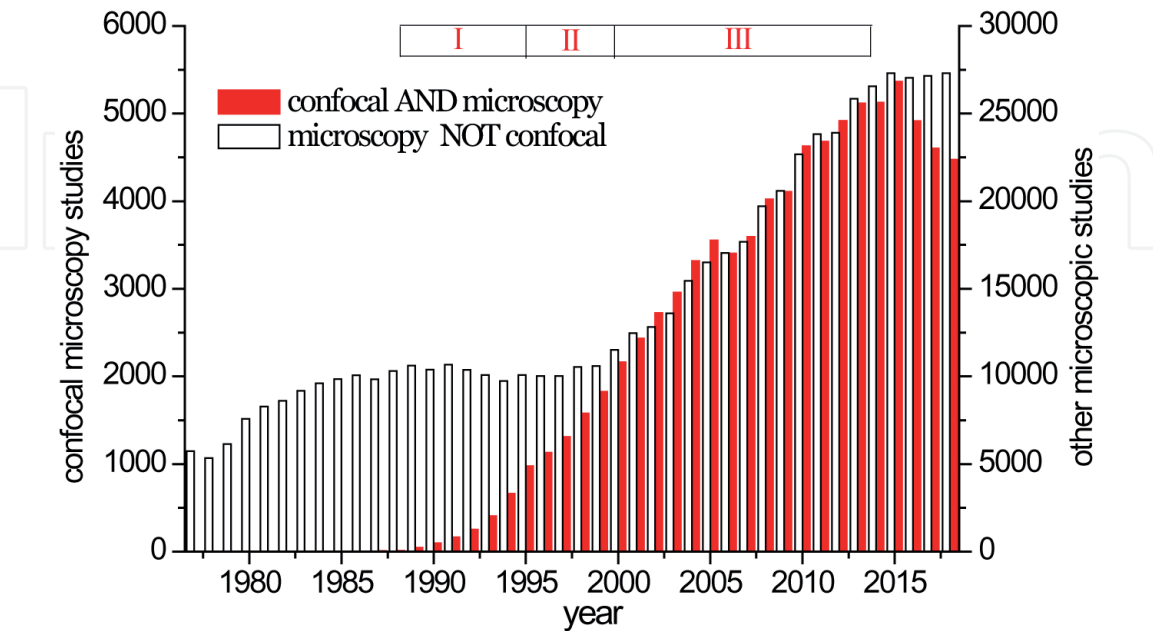


**Figure 1.** Relation between the studies done by confocal or other microscopical methods from 1972 to 2018 following the records from PubMed. Trends of publications by year were downloaded from PubMed web page [27] after placing queries: “confocal and microscopy” and “confocal not microscopy” and pressing the button “timeline” if necessary. Three periods in CLSM development are marked on the graph (see text for discussion).

In real confocal microscope, the detector pinhole determines its axial resolution. The difference in axial resolution between confocal and conventional microscopy can be demonstrated using thin fluorescent sheet. By switching microscope to epi-fluorescent mode, no changes in fluorescence intensity are observed upon moving the test object out of focus. Back to the confocal microscopy mode, fluorescence intensity will decrease in sigmoid manner, the slope of which will depend on pinhole diameter [14]. Thickness of optical section is then given by the formula

$$\text{FWHM} = \frac{0.67\lambda_{ex}}{n - \sqrt{n^2 - NA^2}} \sqrt{1 + AU^2} \quad (2)$$

where  $n$  is the refractive index of immersion medium ( $n = 1.52$ ),  $NA$  is the numerical aperture of objective lens, and  $AU$  is the pinhole diameter in Airy units (or simply “Airy”). Eq. (2) predicts that FWHM of optical section will increase from 0.47 to 1.06  $\mu\text{m}$  by changing  $AU$  from 1 to 3 units. Similarly changing  $AU$  from 1 to 0.6 units will decrease FWHM from 0.47 to 0.39  $\mu\text{m}$ , i.e., by 0.08  $\mu\text{m}$ . These theoretical calculations almost coincide with the data obtained in the real test.

In the current study, we use a step-function fluorescent object for testing the limits of axial resolution of CLSM. The test object was prepared as described in [14] but with the following modifications. Fluoroshield™ mounting media containing 20  $\mu\text{g}/\text{ml}$  rhodamine 6G was placed between a microscopic slide and 24 mm squire coverslip and left under 1 kg weight until drying. Fluorescence intensity profiles were obtained by scanning fluorescent object in X,Z direction at different pinhole sizes. As shown in **Figure 2A**, an increase of pinhole diameter from 1.05 to 3.0 Airy widens fluorescence intensity profile and fluorescence background. Taking the advantage of normal distribution of fluorescence values, we use Gauss function for obtaining FWHM values of intensity curves. The effect of pinhole diameter ranging from 0.45 to 4 Airy units on profile width is presented in **Figure 2B**.

Changes of profile width are correlated with the changes in the optical thickness upon variation of pinhole diameter up to the 3 Airy units. Namely, changing of the pinhole diameter from 1.05 to 3 Airy units increases the width of intensity profile by 0.6  $\mu\text{m}$ . Changing pinhole in reverse order, from 1.05 to 0.65 Airy units, decreases the width of intensity profile by 0.1  $\mu\text{m}$  (**Figure 2B**).

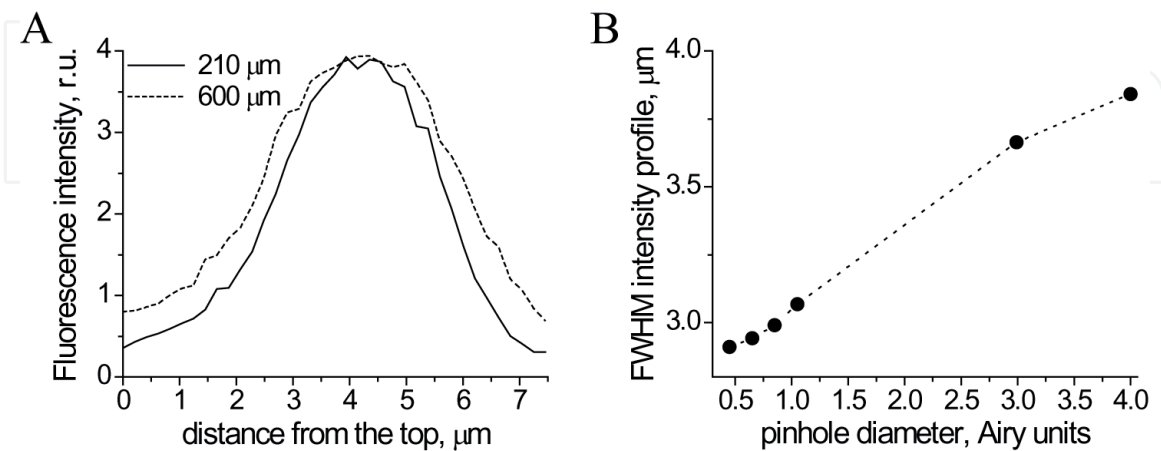


**Figure 2.** Effect of pinhole diameter on the width of fluorescence profile recorded across a layer of Fluoroshield™ media containing 20  $\mu\text{g}/\text{ml}$  rhodamine G. (A) Fluorescent intensity profiles of X,Z optical sections are registered by Olympus FV3000 confocal microscope equipped with 60x/1.42 plan apochromat objective. Fluorescence was excited at 488 nm and collected from 500 to 600 nm. Two fluorescent profiles obtained at pinhole diameters of 210 and 600  $\mu\text{m}$  (corresponding to 1.05 and 3 Airy units) are shown. One curve is the mean of seven plots generated using ImageJ program. Fluorescence intensity is kept constant by adjustment of laser power. (B) FWHM is derived from the intensity profiles obtained at pinhole diameters of 0.45, 0.65, 0.8, 1.05, 3, and 4 Airy units.



The absolute resolution values are usually different from those predicted by Eqs. (1) and (2). Practically it is determined by the measurement of PSF, which is generated by microspheres with a diameter of 170 nm in lateral and axial planes. In one practical study, FWHM was determined as 0.32 and 1.9  $\mu\text{m}$  in X,Y or X,Z directions, respectively [18]. The high value of axial FWHM depth is explained by the necessary use of high pinhole diameter in a study of mitochondrial pH in MDCK cells. Pinhole diameter of about three Airy units was applied in this study to attenuate laser power and minimize its photo-damaging effect on living cells [18, 28].

The resolution of CLSM in large extent depends on the quality of objective lens. Using the correct objective in CLSM is especially important because lens parameters are assumed in the design of particular confocal system. Choosing lens with the same nominal parameters but designed for other microscopes results in more than twice a decrease of resolution [29]. In addition, high-magnification oil-immersion objectives work correctly in media with the refractive index being very close to the refractive index of living cells. Any mismatch of the refractive index decreases the quantity of excited fluorescence and, therefore, resolution of confocal system. Water immersion objectives allow working with deeply lying cells [30].

### **3. Using CLSM in studies of mitochondria**

Earlier confocal systems have difficulties in using multiple dyes. Therefore, studies were done in parallel samples assuming that experimental conditions equally apply for both dyes. SNARF-1 (seminaphthorhodafluor-1, free form) was used for the study of pH of luminal solution along colon crypt. Using CLSM localization SNARF-1 was compared with the localization of dye Lucifer yellow [30]. Pseudo-ratiometric approach utilizes cells stained simultaneously with two dyes localized in the same cellular compartment. MitoTracker Green (MTG) resides in the mitochondria and therefore can be colocalized with the dye of interest [16–18]. As the latter were used one of the following dyes, Rhod-2 (AM), CoroNa Red, or SNARF-1 (AM), accumulated in the mitochondria and giving information on cytoplasmic concentrations of  $[\text{Na}^+]_m$ ,  $[\text{Ca}^{2+}]_m$ , and  $\text{pH}_m$ , respectively. By using Fura-2 (AM), it was shown that during metabolic inhibition, the main source for transient increase in cytoplasmic  $\text{Ca}^{2+}$  concentration ( $[\text{Ca}^{2+}]_c$ ) is the mitochondria [16], and only functionally active mitochondria can have buffering capacity to  $\text{Ca}^{2+}$  [31].

A large number of studies are directed to understand mitochondrial heterogeneity, which is manifested as the differences in shape and size of the mitochondria in a single cell [8, 9] or morphological differences between cell types [32]. Some cell mitochondria appear as network but in others as discrete individuals [32]. Fission and fusion that maintain the dynamic structure of mitochondrial network are mechanisms involved in the regulation of cell proliferation and apoptosis [33]. These processes are sensitive to cell metabolic state and MMP. Elongated mitochondria are dominant in mouse embryonic fibroblasts grown in conditions promoting oxidative phosphorylation. The addition of glucose suppresses elongation and causes fragmentation [34]. In the study, reviewed in the next section, the attempt was made to uncover the dynamic nature of MMP changes and its role in maintaining mitochondrial network structure.

### **4. Using CLSM in quantitative MMP studies**

In studies of MMP, it is important to consider the thickness of optical section because it determines the affectivity of detection of mitochondrial fluorescence.

FWHM of optical section that is calculated by Eq. (2) is almost fit to the dimensions of the mitochondria in U937 cells. Electron microscopic studies follow that the mitochondria in U937 cells are spheroidal in structures with a diameter of 0.6–0.8  $\mu\text{m}$  [35]. Therefore, CLSM is effectively collecting fluorescence from the mitochondria of TMRE-stained U937 cells. The mitochondria in lymphocytes have a diameter of only 0.3–0.4  $\mu\text{m}$  [19, 36, 37], and the affectivity of collection of mitochondrial fluorescent signal is less than U937 cells. The mitochondrial shape is also considered in choosing the right procedure for image processing. Thus, different procedures are required for the study of mitochondria in U937 cells or in skin fibroblasts having threadlike appearance [38].

Using CLSM in the study of MMP, it is possible to select for analysis the whole cell area. This selection includes nonmitochondrial compartment that constitutes about 95–98% of the total cell volume [10, 20]. Its signal can be set as a background and subtracted from total fluorescence. The example of this approach is found in a study of MMP changes in lamprey hepatocytes during prespawning migration. As can be expected, CLSM gave results similar to that of flow cytometry [39]. The reason why this approach is chosen by authors is the absence of parallel control samples that are necessary for analytical procedures involving image processing.

Another simplified approach is based on staining of cells with TMRE and MTG and using MTG as reference. For example, TMRE/MTG fluorescence ratio was decreased in the muscle cells of zebrafish embryo after chronical treatment by rotenone [40]. The utilization of MTG as reference dye however is limited because its uptakes in some types of cells depend on MMP [41]. Therefore, MTG is generally used for the creation of mask [16–18]. By combination of these approaches, it was shown that both TMRE/MTG ratio and MTG signal increased during malignant transformation of mesenchymal stem cells [10].

Good substitute for MTG is mitochondria-specific green fluorescence proteins (GFP). MitoAcGFP1 located in mitochondrial matrix was used for the study of mitochondrial  $[\text{Ca}^{2+}]_m$  [6]. Photoactivatable GFP was used for tracking individual mitochondria in order to relate their MMP to fission events [42, 43]. Data obtained in later studies lead authors to the conclusion that depolarization triggers fission of the mitochondria and fission serves as the quality control for its functional properties [43]. However, the applicability of GFP is limited by insufficient level of expression in some cell types [32, 42]. Rhodamine ester dyes were also used as reference dye in the study of  $[\text{Ca}^{2+}]_m$  [31]. Evidence was provided that TMRM (tetramethylrhodamine, methyl ester) is not liable to auto-quenching and therefore suitable both for the creation of mask and determination of MMP [6]. This is especially important because data obtained using dye rhodamine 123 do not allow their interpretation in terms of MMP.

CLSM experiments with living cells are preceded by cell staining. During staining, TMRE dye almost completely uptakes the cells; hence, it is important to keep constant the dye-to-cell ratio. This ratio should also be equal in control and treated cells. During image acquisition it is possible to use previously saved settings. The function of “auto-exposure” can be used only once with living cells at the beginning of the study [44]. The reason for this is to keep cells from overexposure from laser irradiation. The optimum settings however allow keeping the dynamic range of detector maximum and preventing most of the pixel on image from saturation. Fluorescence intensity is almost linearly dependent on laser power and nearly exponentially—on voltage of photomultiplier tube (PMT). Therefore, it is generally recommended to set PMT voltage first and then adjust laser excitation intensity [44]. With calibration, PMT voltage also can be varied and used for adjustment [18, 28].

## 5. Digital image processing in quantitative MMP studies

Examples of image processing that can be found in the earliest studies are threshold, gradient filtering, and segmentation. These procedures are applied to images resulted from summing of intensity along the Z-axis [26]. Graphical filters are specific instruments used to eliminate noise or other unwanted information from image. “Rolling ball” algorithm uses rank operators to remove pixels exceeding the local background level and replaces them with pixels of neighborhood intensity. The processed image is then subtracted from the original image [45]. “Top hat” filter is used for processing such complex structures as mitochondrial network in human skin fibroblast [8, 9]. “Rolling ball” filter is suitable for images of U937 cells containing the mitochondria of elliptical shape.

### 5.1 Image processing in quantitative MMP studies

For demonstration of image processing in our study, U937 cells were treated with PHA (30  $\mu\text{g/ml}$ , 2 h) and stained with 25 nM of TMRE dye. Cell suspension was placed in Plexiglas holder and scanned in the middle plane of the most cells. Histogram equalization was used to check the amount of TMRE in nonmitochondrial compartment. This was done by running command “enhance contrast” in ImageJ program. Apart from the mitochondria and cytoplasm, small fluorescence is present in the nucleus (**Figure 3A and B**). To remove background fluorescence, images were processed by “subtract background” algorithm in ImageJ program that utilizes “rolling ball” operator [46]. On the next step, the processed image is subjected to thresholding, which is used to suppress variations at the background level [45]. ImageJ program allows obtaining quantitative data after setting a threshold and execution of commands “create selection” and “analyze stack.” However,

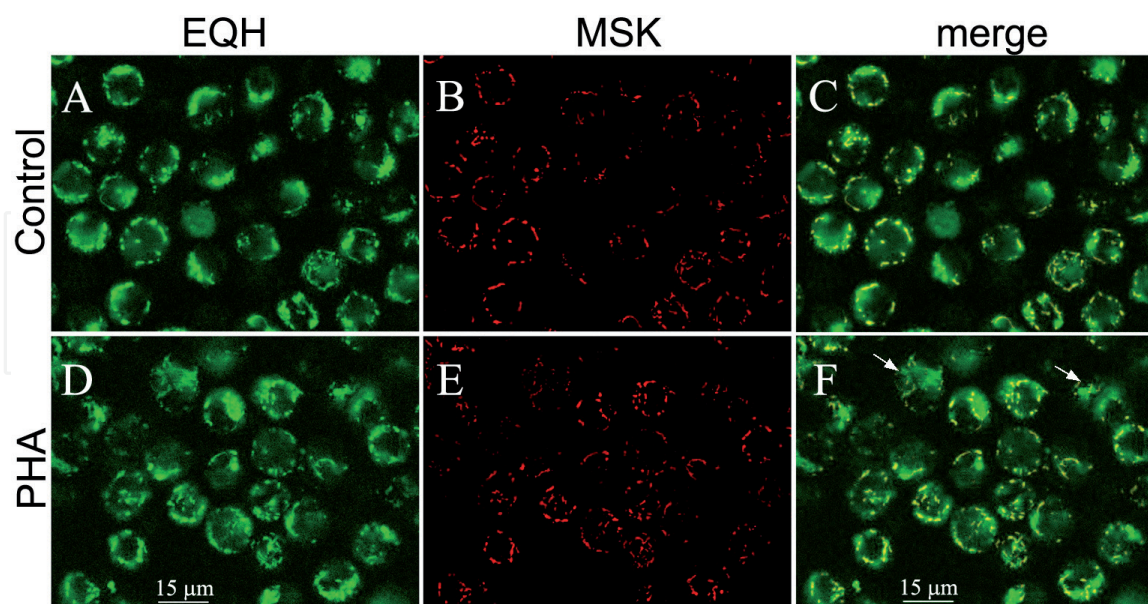


**Figure 3.**

*Demonstration of using image processing for quantitative study of MMP changes in U-937 cell during PHA treatment. Cells were incubated without (A–C) or with p-PHA (30  $\mu\text{g/ml}$ ) for 2 h (D–F) in atmosphere of 5%  $\text{CO}_2$  and stained with 25 nM TMRE for 30 min at 37°C. Excess of media was removed by centrifugation. 20  $\mu\text{l}$  of cell suspension is placed on coverslip and a 1% gelatin solution is attached to Plexiglas holder sealed from another side with coverslip. Fluorescence was excited by 561 nm diode laser and collected at 575–675 nm through pinhole of 178 nm (0.73 Airy units). (A, D), raw images after histogram equalization (EQH); (B, E), masked version of this images (MSK); (C, F), merged images of MSK (red pseudo-color), and EQH (green pseudo-color). Red pixels colocalized with green pixels in an area of high intensity except the blurred regions that are present in some cells. Arrows indicate small aggregates of agglutinated cells.*



for demonstration of validity of this procedure, binary mask (mask) was applied to histogram-equalized image (HEQ) rather than to original image (RAW). This operation gives possibility to see variations within regions, which appeared uniform in the original image [45]. The procedure of histogram equalization is similar to the linear contrast stretch used in other works [6]. The resulting masked images (MSK) contain nonzero pixels that correspond to mitochondrial compartment (**Figure 3B** and **E**). Histogram equalization emphasizes mitochondrial heterogeneity and proves the absence of fluorescence in cytoplasmic compartment. However, HEQ images do not give possibility to see the difference of intensities between control- and PHA-treated cells because changes of intensity caused by this procedure are specific to each image [45].

Using merged images it is possible to see similarity between MSK and nonzero regions of HEQ image. As it can be seen in **Figure 3C** and **F**, colocalization is present in all regions except blurred parts that are present in both control- and PHA-treated cells. Good correlation between MSK and HEQ is also seen by “Color inspector 3D” plug-in in ImageJ program. The presence of cell groups that mark the beginning of agglutination process was noticed on the image of PHA-treated cells (**Figure 3F**, arrows). At this period, however, agglutinated cells are lying in plane of imaging available for study.

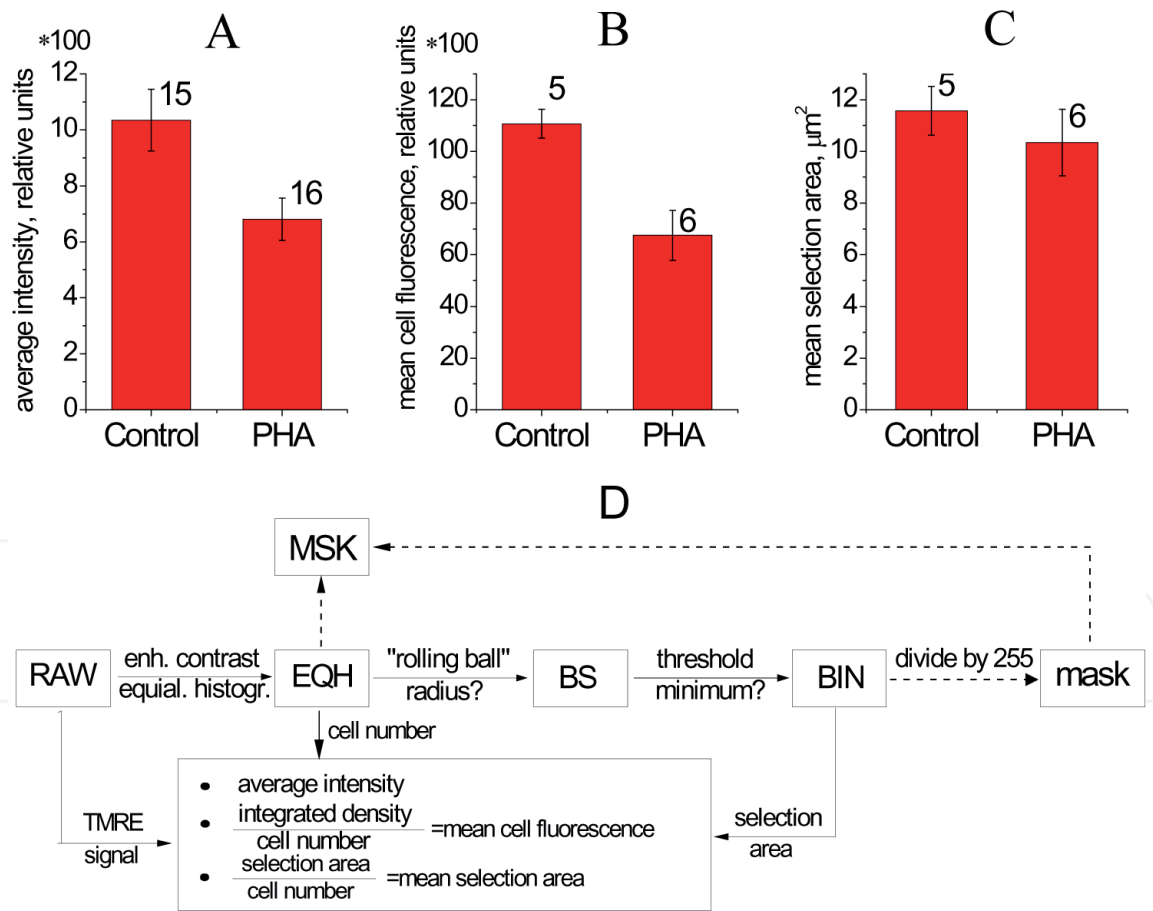


**Figure 4.** Quantification of MMP changes in U937 cells during PHA treatment (30  $\mu\text{g}/\text{ml}$ , 2 h). (A–C) quantitative data retrieved from images acquired in one (B, C) and three (A) experiments. Data are expressed as means  $\pm$  SD. The number of images that is used in the analysis is shown near each bar. (A) Average TMRE fluorescence intensity found in selection area. (B) Mean cell fluorescence calculated as integrated density divided by the number of cells. (C) Mean area of selection calculated as total selection area divided by the number of cells. (D) Protocol of imaging processing and analysis. Most important operations are shown by arrows, while its results are indicated in boxes: RAW, original image; EQH, original image after histogram equalization; BS and BIN, images after running “subtracted background” and “threshold” commands, respectively; mask, mask image; MSK, image obtained by multiplying EQH image by mask image. Dot lines show the operations used for the creation of masked image (MSK).

## 5.2 Study of MMP changes during PHA stimulation

For quantitative analysis of MMP changes, two analytical values were used. Average intensity is a measure of absolute MMP, but it underestimates changes of MMP if they occur below the threshold level (**Figure 4A**). The relative value is obtained by the division of integrated density to cell number considering the presence of cells with completely depolarized MMP. This value is applied more specifically and therefore was named “mean cell fluorescence” (**Figure 4B**). The decrease of average intensity caused by PHA treatment is lower than the corresponding decrease of mean cell fluorescence by 5%. This dissimilarity shows the presence of cells whose fluorescence changed below the detection limit. The changes in the selection area are calculated as the total selection area on images divided by the number of cells attributing to these fluorescent images (**Figure 4C**).

The relation between these analytical options can be understood from the schematic representation of full analytical process shown in **Figure 4D**. It started from original image (RAW), the duplicate of which passes three steps until it resulted in the generation of mask or the selection of congruent regions on RAW image with output of numerical results. Histogram equalization, background subtraction, and thresholding were done similarly to those published in earlier works [6, 28]. The method presented in **Figure 4D** also gives possibility to control mitochondrial selection area and compare it with already known morphological data. From the data presented in **Figure 4C** and from known value of cell area ( $120 \mu\text{m}^2$ ), it can be concluded that selected area constitutes about 10% of cell area. This is close, for example, to a value of 8% in tumorigenic cell lines obtained by electron-microscopic examination [10].

## 6. Role of mitochondria in response of lymphoid cells to PHA treatment

The decrease of average fluorescence intensity by 34% after 2 h of PHA treatment is attributed to the changes of absolute MMP value. While our data were obtained on the early stage of stimulation, they can be correlated with data on metabolic shift that occurs in lymphoid cells after prolonged treatment. These data suggest that the role of the mitochondria in total energy balance decreases during stimulation. It was shown that glycolytic activity in lymphocytes increases by 36 times but the respiratory activity is only by 43% [21]. In thymocytes that obtain energy mainly by glucose oxidation, lectin treatment leads to the deceleration of this pathway [47]. On the contrary, in mesenchymal stem cell, mitochondrial activity is increased during malignant transformation [10].

The difference in selection area between control- and PHA-treated cells (**Figure 4C**) suggests that MMP in some cells is completely lost. These changes could be related to the changes of  $[\text{Ca}^{2+}]_c$  because it is known that  $[\text{Ca}^{2+}]_c$  is increased after mitogenic stimulation [48]. The mitochondria play essential role in the regulation of  $[\text{Ca}^{2+}]_c$  [31, 49]. During metabolic inhibition in MDCK cells,  $[\text{Ca}^{2+}]_c$  is transiently increased. Restoration of normal  $[\text{Ca}^{2+}]_c$  occurs by coupled action mitochondrial  $\text{Na}^+/\text{Ca}^{2+}$  and  $\text{Na}^+/\text{H}^+$  exchangers. Metabolic inhibition decreases proton gradient on mitochondrial membrane [18] and reduces outward  $\text{Na}^+$  and  $\text{Ca}^{2+}$  movement mediated by these transporters. As a consequence,  $\text{Na}^+$  and  $\text{Ca}^{2+}$  concentration in mitochondrial matrix is steadily increased [16, 17].

Similar situation may exist in stimulated lymphoid cells where the magnitude of proton electrochemical gradient is compromised by the changes of  $\text{pH}_c$ . The  $\text{Na}^+$  content in lymphocytes is increased rapidly after PHA treatment with maximum of 2 h [50]. Both  $\text{K}^+$  content and influx are also increased during mitogenic stimulation [50].

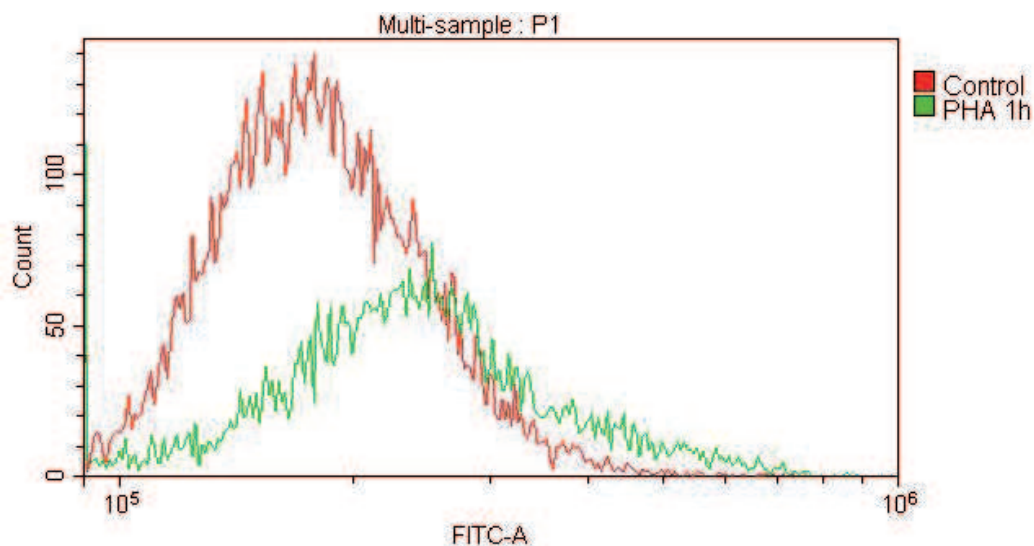


**Figure 5.**

Effect of PHA treatment (30  $\mu\text{g/ml}$ , 1 h) on fluorescence of ANG dye. Cells stained with ANG-AM (1  $\mu\text{M}$ ) during the last 40 min of PHA treatment (37°C). ANG fluorescence was excited using a 488 nm laser, and emission was detected in the FITC channel with a 525/40 nm bandpass. Data were analyzed using CytExpert 2.0 Beckman Coulter software. The major cell populations were selected for analysis using forward/side scatter plot. Data were obtained using the same samples as data presented in **Figures 3 and 4B and C**.

Therefore, the increase of cytoplasmic  $[\text{Na}^+]_c$  in response to lectin treatment is mediated by  $\text{Na}^+/\text{H}^+$  exchanger. This view agrees with the increase of  $\text{pH}_c$  in both thymocytes and lymphocytes after lectin treatment [51, 52]. To test whether these changes take place in U937 cells during PHA stimulation, we performed investigation of  $[\text{Na}^+]_c$  by Na-sensitive dye Asante Natrium Green-2 (ANG). As followed from the flow cytometric data, the fluorescence of ANG was increased after 1 h of PHA treatment (**Figure 5**). The mean ANG fluorescence increased by PHA treatment from  $1.89\text{E}+05$  to  $2.59\text{E}+05$  relative units. Assuming that changes of fluorescence are proportional to the changes of concentration,  $[\text{Na}^+]_c$  will increase from 30 mM in resting U937 cells to 38 mM upon PHA treatment.

The demonstrated increase of  $[\text{Na}^+]_c$  in PHA-stimulated U937 cells may be considered as part of the regulatory mechanism involved in the increase of  $[\text{Ca}^{2+}]_m$ . The increase of  $[\text{Ca}^{2+}]_m$  in many cell types causes activation of mitochondrial dehydrogenases [49] and accounts for the rapid activation of mitochondrial PDH in response to lectin action [23, 53]. The increase of  $[\text{Ca}^{2+}]_m$  can also lead to mitochondrial injury that was confirmed by serious ultra-structural changes observed in human lymphocytes after 3 days of lectin treatment [36, 54]. The deleterious effect of lectins on mitochondrial morphology, however, was absent in other experiments [19, 37, 54]. Controversy of results obtained in these studies can be explained by the complexity of regulatory mechanisms controlling mitochondrial  $\text{Ca}^{2+}$  and  $\text{Na}^+$  homeostasis. This reason can also be applied in our study in which a large variation in the number of cells with complete mitochondrial depolarization was noticed.

## 7. Conclusions

The role of the mitochondria in energy supply is determined by the functional state of the cells. This problem is usually addressed by biochemical, polarographic and optical methods which measure ATP production and oxygen consumption in the living cell. In many studies, it is also corroborated by parallel measurement of mitochondrial membrane potential (MMP). This article describes fluorescent

method of measuring MMP in cancer cell using potential-sensitive dye TMRE. This method can distinguish fluorescence of TMRE in mitochondrial and nonmitochondrial compartment by using standard software for image analysis.

## Acknowledgements

I acknowledge TS Goryachaya for maintaining a cell culture and ND Aksenov for assistance with flow cytometry investigations. I am very grateful to JP Battersby for discussions leading to the current study and to GI Shtein for technical consultations. I am also thankful to Prof. VS Saakov for his help in the writing of this manuscript.


## Author details

Alexey Moshkov

Institute of Cytology of Russian Academy of Sciences, St. Petersburg, Russia

\*Address all correspondence to: [moshov\\_alexey@mail.ru](mailto:moshov_alexey@mail.ru)

## IntechOpen

© 2020 The Author(s). Licensee IntechOpen. Distributed under the terms of the Creative Commons Attribution - NonCommercial 4.0 License (<https://creativecommons.org/licenses/by-nc/4.0/>), which permits use, distribution and reproduction for non-commercial purposes, provided the original is properly cited. 



## References

- [1] Frank GM, Tigyi J, Shnol SE, Bauer ES, editors. *Theoretical Biology* (Reprint of 1935 Edition with Preface, a Biographical and Critical Essay). Budapest: Akadémiai Kiadó; 1982. p. 295
- [2] Keynes RD, Lewis PR. The sodium and potassium content of cephalopod nerve fibers. *The Journal of Physiology*. 1951;**114**:151-182. DOI: 10.1113/jphysiol.1951.sp004609
- [3] Lacey AJ. Basic optical microscopy. In: Lacey AJ, editor. *Light Microscopy in Biology. A Practical Approach*. 2nd ed. New York: Oxford University Press; 1999. pp. 1-43
- [4] Van Hulst NF. Near-field optical microscopy. In: Lacey AJ, editor. *Light Microscopy in Biology: A Practical Approach*. 2nd ed. New York: Oxford University Press; 1999. pp. 341-371
- [5] Hwang J, Gheber LA, Margolis L, Edidin M. Domains in cell plasma membranes investigated by near-field scanning optical microscopy. *Biophysical Journal*. 1998;**74**:2184-2190. DOI: 10.1016/S0006-3495(98)77927-5
- [6] Distelmaier F, Koopman WJ, Testa ER, de Jong AS, Swarts HG, Mayatepek E, et al. Life cell quantification of mitochondrial membrane potential at the single organelle level. *Cytometry. Part A*. 2008;**73**:129-138. DOI: 10.1002/cyto.a.20503
- [7] Koopman WJ, Distelmaier F, Esseling JJ, Smeitink JA, Willems PH. Computer-assisted live cell analysis of mitochondrial membrane potential, morphology and calcium handling. *Methods*. 2008;**46**:304-311. DOI: 10.1016/j.ymeth.2008.09.018
- [8] Koopman WJ, Verkaart S, Visch HJ, et al. Inhibition of complex I of the electron transport chain causes O<sub>2</sub><sup>-•</sup>-mediated mitochondrial outgrowth. *American Journal of Physiology. Cell Physiology*. 2005;**288**:C1440-C1450. DOI: 10.1152/ajpcell.00607.2004
- [9] Koopman WJ, Visch HJ, Smeitink JA, Willems PH. Simultaneous quantitative measurement and automated analysis of mitochondrial morphology, mass, potential, and motility in living human skin fibroblasts. *Cytometry. Part A*. 2006;**69**:1-12. DOI: 10.1002/cyto.a.20198
- [10] Lonetto G, Koifman G, Silberman A, Attery A, Solomon H, Levin-Zaidman S, et al. Mutant p53-dependent mitochondrial metabolic alterations in a mesenchymal stem cell-based model of progressive malignancy. *Cell Death and Differentiation*. 2019;**26**:1566-1581. DOI: 10.1038/s41418-018-0227-z
- [11] Weiss DG. Video microscopy. In: Lacey AJ, editor. *Light Microscopy in Biology: A Practical Approach*. 2nd ed. New York: Oxford University Press; 1999. pp. 73-149
- [12] Shaw PJ. Comparison of widefield/deconvolution and confocal microscopy for three-dimensional imaging. In: Pawley JB, editor. *Handbook of Biological Confocal Microscopy*. 3d ed. Boston: Springer; 2006. pp. 453-467. DOI: 10.1007/978-0-387-45524-2\_23
- [13] Deng X, Zhironkina OA, Cherepanynets VD, Strelkova OS, Kireev II, Belmont AS. Cytology of DNA replication reveals dynamic plasticity of large-scale chromatin fibers. *Current Biology*. 2016;**26**:2527-2534. DOI: 10.1016/j.cub.2016.07.020
- [14] Amos B, McConnell G, Wilson T. Chapter 2.2: Confocal Microscopy. In: Egelman E, editor. *Comprehensive Biophysics*. 1st ed. Amsterdam: Elsevier;

2012. pp. 3-23. DOI: 10.1016/B978-0-12-374920-8.00203-4

[15] Shaw PJ. Introduction to confocal microscopy. In: Lacey AJ, editor. *Light Microscopy in Biology: A Practical Approach*. 2nd ed. New York: Oxford University Press; 1999. pp. 45-71

[16] Smets I, Caplanusi A, Despa S, Molnar Z, Radu M, VandeVen M, et al.  $\text{Ca}^{2+}$  uptake in mitochondria occurs via the reverse action of the  $\text{Na}^+/\text{Ca}^{2+}$  exchanger in metabolically inhibited MDCK cells. *American Journal of Physiology. Renal Physiology*. 2004;**286**:F784-F794. DOI: 10.1152/ajprenal.00284.2003

[17] Baron S, Caplanusi A, van de Ven M, Radu M, Despa S, Lambrichts I, et al. Role of mitochondrial  $\text{Na}^+$  concentration, measured by CoroNa red, in the protection of metabolically inhibited MDCK cells. *Journal of the American Society of Nephrology*. 2005;**16**:3490-3497. DOI: 10.1681/ASN.2005010075

[18] Balut C, van de Ven M, Despa S, Lambrichts I, Ameloot M, Steels P, et al. Measurement of cytosolic and mitochondrial pH in living cells during reversible metabolic inhibition. *Kidney International*. 2008;**73**:226-232. DOI: 10.1038/sj.ki.5002632

[19] Marshall WH, Roberts KB. The growth and mitosis of human small lymphocytes after incubation with a phytohaemagglutinin. *Quarterly Journal of Experimental Physiology and Cognate Medical Sciences*. 1963;**2**:146-155. DOI: 10.1113/expphysiol.1963.sp001645

[20] Brand MD, Felber SM. Membrane potential of mitochondria in intact lymphocytes during early mitogenic stimulation. *Biochemical Journal*. 1984;**217**:453-459. DOI: 10.1042/bj2170453

[21] Pachman LM. The carbohydrate metabolism and respiration of isolated

small lymphocytes. In vitro studies of normal and phytohemagglutinin stimulated cells. *Blood*. 1967;**30**:691-706. DOI: 10.1182/blood.V30.6.691.691

[22] Hedeskov CJ. Early effects of phytohemagglutinin on glucose metabolism of normal human lymphocytes. *Biochemical Journal*. 1968;**110**:373-380. DOI: 10.1042/bj1100373

[23] Beachy JC, Goldman D, Czech MP. Lectins activate lymphocyte pyruvate dehydrogenase by a mechanism sensitive to protease inhibitors. *Proceedings of the National Academy of Sciences of the United States of America*. 1981;**78**:6256-6260. DOI: 10.1073/pnas.78.10.6256

[24] Minsky M. Memoir on inventing the confocal scanning microscope. *Scanning*. 1988;**10**:128-138. DOI: 10.1002/sca.4950100403

[25] White JG, Amos WB. Confocal microscopy comes of age. *Nature*. 1987;**328**:183-184. DOI: 10.1038/328183a0

[26] Aslund N, Liljeborg A, Forsgren PO, Wahlsten S. Three-dimensional microscopy using the PHOIBOS scanner. *Scanning*. 1987;**9**:227. DOI: 10.1002/sca.4950090603

[27] PubMed [Internet]. Bethesda, MD: National Library of Medicine (US). 1946. Available from: <https://www.ncbi.nlm.nih.gov/pubmed/> [Accessed: 10 March 2020]

[28] van de Ven M, Balut C, Baron S, Smets I, Steels P, Ameloot M. Analysis of mitochondrial pH and ion concentrations. *Methods in Molecular Biology*. 2010;**591**:275-309. DOI: 10.1007/978-1-60761-404-3\_17

[29] Zucker R. Confocal microscopy system performance: Axial resolution. *Microscopy Today*. 2004;**12**:38. DOI: 10.1017/S1551929500051816

- [30] Chu S, Brownell WE, Montrose MH. Quantitative confocal imaging along the crypt-to surface axis of colonic crypts. *American Journal of Physiology. Cell Physiology*. 1995;**269**:C1557-C1564. DOI: 10.1152/ajpcell.1995.269.6.C1557
- [31] McKenzie M, Duchen MR. Impaired cellular bioenergetics causes mitochondrial calcium handling defects in MT-ND5 mutant cybrids. *PLoS One*. 2016;**11**:e0154371. DOI: 10.1371/journal.pone.0154371
- [32] Collins TJ, Bootman MD. Mitochondria are morphologically heterogeneous within cells. *Journal of Experimental Biology*. 2003;**206**:1993-2000. DOI: 10.1242/jeb.00244
- [33] Rehman J, Zhang HJ, Toth PT, Zhang Y, Marsboom G, Hong Z, et al. Inhibition of mitochondrial fission prevents cell cycle progression in lung cancer. *The FASEB Journal*. 2012;**26**:2175-2186. DOI: 10.1096/fj.11-196543
- [34] Mishra P, Carelli V, Manfredi G, Chan DC. Proteolytic cleavage of Opa1 stimulates mitochondrial inner membrane fusion and couples fusion to oxidative phosphorylation. *Cell Metabolism*. 2014;**19**:630-641. DOI: 10.1016/j.cmet.2014.03.011
- [35] Snigirevskaya ES, Moshkov AV, Yurinskaya VE, Vereninov AA, Komissarchik YY. Ultrastructural and X-ray microanalysis of U-937 cells in hypertonia-induced apoptosis. *Cell and Tissue Biology*. 2015;**9**:96-109. DOI: 10.1134/S1990519X15020091
- [36] Inman DR, Cooper EH. Electron microscopy of human lymphocytes stimulated by phytohaemagglutinin. *Journal of Cell Biology*. 1963;**19**:441-445. DOI: 10.1083/jcb.19.2.441
- [37] Johnson FR, Roberts KB. The growth and division of human small lymphocytes in tissue culture: An electron microscopic study. *Journal of Anatomy*. 1964;**98**:303-311
- [38] Koopman WJ, Distelmaier F, Hink MA, Verkaart S, Wijers N, Fransen J, et al. Inherited complex I deficiency is associated with faster protein diffusion in the matrix of moving mitochondria. *American Journal of Physiology. Cell Physiology*. 2008;**294**:C1124-C1132. DOI: 10.1152/ajpcell.00079.2008
- [39] Savina MV, Konovalova SA, Zubatkina IS, Nikiforov AA. Reversible metabolic depression in lamprey hepatocytes during prespawning migration: Dynamics of mitochondrial membrane potential. *Comparative Biochemistry and Physiology Part B: Biochemistry and Molecular Biology*. 2011;**160**:194-200. DOI: 10.1016/j.cbpb.2011.08.007
- [40] Byrnes J, Ganetzky R, Lightfoot R, Tzeng M, Nakamaru-Ogiso E, Seiler C, et al. Pharmacologic modeling of primary mitochondrial respiratory chain dysfunction in zebrafish. *Neurochemistry International*. 2018;**117**:23-34. DOI: 10.1016/j.neuint.2017.07.008
- [41] Buckman JF, Hernandez H, Kress GJ, Votyakova TV, Pal S, Reynolds IJ. MitoTracker labeling in primary neuronal and astrocytic cultures: Influence of mitochondrial membrane potential and oxidants. *Journal of Neuroscience Methods*. 2001;**104**:165-176. DOI: 10.1016/S0165-0270(00)00340-X
- [42] Twig G, Graf SA, Wikstrom JD, Mohamed H, Haigh SE, Elorza A, et al. Tagging and tracking individual networks within a complex mitochondrial web with photoactivatable GFP. *American Journal of Physiology. Cell Physiology*. 2006;**291**:C176-C184. DOI: 10.1152/ajpcell.00348.2005



- [43] Twig G, Elorza A, Molina AJ, et al. Fission and selective fusion govern mitochondrial segregation and elimination by autophagy. *EMBO Journal*. 2008;**27**:433-446. DOI: 10.1038/sj.emboj.7601963
- [44] Brown CM. Fluorescence microscopy—Avoiding the pitfalls. *Journal of Cell Science*. 2007;**120**:1703-1705. DOI: 10.1242/jcs.03433
- [45] Russ JC. The Image Processing Handbook. 3d ed. Boca Raton: CRC Press; 1999. p. 771
- [46] Ferreira T, Rasband WS. ImageJ User Guide IJ1.46r [Internet]. Available from: <https://imagej.nih.gov/ij/docs/guide/146-29.html#sub:Subtract-Background...> [Accessed: 18 April 2020]
- [47] Brand KA, Hermfisse U. Aerobic glycolysis by proliferating cells: A protective strategy against reactive oxygen species. *FASEB Journal*. 1997;**11**:388-395. DOI: 10.1096/fasebj.11.5.9141507
- [48] Whitney RB, Sutherland RM. Characteristics of calcium accumulation by lymphocytes and alterations in the process induced by phytohemagglutinin. *Journal of Cellular Physiology*. 1973;**82**:9-20. DOI: 10.1002/jcp.1040820103
- [49] Denton RM, McCormack JG. On the role of the calcium transport cycle in heart and other mammalian mitochondria. *FEBS Letters*. 1980;**119**:1-8. DOI: 10.1016/0014-5793(80)80986-0
- [50] Marakhova II, Vereninov AA, Toropova FV, Vinogradova TA. Na, K-ATPase pump in activated human lymphocytes: On the mechanisms of rapid and long-term increase in K influxes during the initiation of phytohemagglutinin-induced proliferation. *Biochimica et Biophysica Acta*. 1998;**1368**:61-72. DOI: 10.1016/s0005-2736(97)00164-8
- [51] Grinstein S, Smith JD, Rowatt C, Dixon SJ. Mechanism of activation of lymphocyte Na<sup>+</sup>/H<sup>+</sup> exchange by concanavalin A. A calcium- and protein kinase C-independent pathway. *Journal of Biological Chemistry*. 1987;**262**:15277-15284
- [52] Chien EJ, Chang CP, Lee WF, Su TH, Wu CH. Non-genomic immunosuppressive actions of progesterone inhibits PHA-induced alkalization and activation in T cells. *Journal of Cellular Biochemistry*. 2006;**99**:292-304. DOI: 10.1002/jcb.20858
- [53] Baumgarten E, Brand MD, Pozzan T. Mechanism of activation of pyruvate dehydrogenase by mitogens in pig lymphocytes. *Biochemical Journal*. 1983;**216**:359-367. DOI: 10.1042/bj2160359
- [54] Douglas SD. Electron microscopic and functional aspects of human lymphocyte response to mitogens. *Immunological Reviews*. 1972;**11**:39-59. DOI: 10.1111/j.1600-065x.1972.tb00045.x